RSC Advances

PAPER

View Article Online
View Journal | View Issue

Cite this: *RSC Adv.*, 2021, **11**, 15808

Roles of water in the formation and preparation of graphene oxide†

Qiang Zhang,[a] Yuying Yang,[a] Huiqing Fan,[a] Liu Feng,[b] Guangwu Wen[b] and Lu-Chang Qin[c]

Received 27th November 2020
Accepted 14th April 2021

DOI: 10.1039/d0ra10026a

rsc.li/rsc-advances

The functional groups and physical properties of graphene oxide (GO) are found to be sensitive to and can be controlled by the water content in the reactions when GO samples are prepared at different concentrations of sulfuric acid using a modified Hummers method. GO prepared with 93% sulfuric acid (H_2SO_4) showed fewer structural defects, less π–π conjugation, and larger interlayer spacing than GO prepared with 99% H_2SO_4. The intensity ratio of the D-band to the G-band of the Raman spectrum is 0.89 ± 0.01 and 1.02 ± 0.01, corresponding to average interlayer spacing of 0.91 nm and 0.86 nm, respectively. The yield and carbon to oxygen ratio of the GO sheets prepared from different concentrations of H_2SO_4 are nearly identical. More importantly, compared with GO synthesized with 99% H_2SO_4, GO prepared with 93% H_2SO_4 contains more carbon–oxygen single bonds, such as epoxy groups and hydroxyl groups, but fewer carbonyl groups.

1. Introduction

Graphene is a two-dimensional material with unique properties,[1] such as mechanical stiffness, superior strength and elasticity, large specific surface area, and exciting potentials for energy storage and nanoelectronics applications.[2–6] Therefore it is of great importance to establish experimental methods for mass-production of graphene with fewer layers and fewer structural defects. Since Stankovich *et al.* reported their successful results to obtain monolayer graphene by oxidation and reduction, the chemical method has become the most widely used technique to prepare graphene.[7,8]

Graphene oxide (GO) is the precursor for preparation of graphene and it can be prepared through several approaches.[9,10] The structure and properties of GO determine the quality and conductivity of graphene.[11] Graphite oxide was first prepared by Brodie in 1859.[12] Hummers and Offeman refined the method in 1958 that has since been widely used for the synthesis of GO.[13] It has been observed and recognized that the product of these reactions was sensitive to not only the particular oxidants used, but also the graphite precursor and reaction conditions.[14,15] This method and other subsequent improved Hummers methods all used sulfuric acid (H_2SO_4) to intercalate graphite and potassium permanganate ($KMnO_4$) as a strong oxidant with the assistance of sodium nitrate ($NaNO_3$) as an activator of aromatic carbon.[16,17] As of today, H_2SO_4 is still the best intercalation solvent for the synthesis of GO.

Graphene has excellent electrical conductivity that relies mainly on the conjugate network of graphitic structure.[18,19] Functional groups are usually attached on the basal plane of reduced graphene oxide (rGO) and the structural defects not only destroy the conjugation, but also localize the π-electrons, which often result in a decrease of both carrier mobility and carrier concentration.[20] Therefore, the reduction of GO is not only concerned with removing the oxygenic functional groups bonded to graphene and atomic-scale lattice defects, but also is aimed at recovering the conjugated network of the graphitic lattice.

According to the mechanism of reduction with hydrazine, hydrazine hydrate ($N_2H_4 \cdot H_2O$) can only reduce the epoxy group, forming a hydroxyl group with a low bonding energy and high activity.[21,22] Then the hydroxyl group would form water molecules at normal temperature. The carbonyl groups and the carboxyl groups would remain present on the edges of the graphene sheet. Therefore, a successful synthesis of GO should satisfy two basic requirements: (a) reduce the carbonyl groups on the basal plane and (b) create structural defects in GO as few as possible to ensure rGO to possess a more graphitic structure with fewer defects. If there are many defects on the surface of GO, such defects would form new edges and then produce carbonyl groups in the oxidation reaction. Marcano *et al.* used a 9 : 1 sulfuric acid (H_2SO_4) and phosphoric acid (H_3PO_4)-mixed solvent to synthesize GO with fewer structural defects and fewer carbonyl functional groups, though this method suffered from a low yield and also introduced phosphorus impurities.[23]

[a]College of Chemistry and Chemical Engineering, Shandong University of Technology, China
[b]College of Materials Science and Engineering, Shandong University of Technology, China
[c]Department of Physics and Astronomy, University of North Carolina at Chapel Hill, China

† Electronic supplementary information (ESI) available. See DOI: 10.1039/d0ra10026a

Kang *et al.* reported the effect of oxidation temperature on the particle size and physical properties of graphite oxide sheets.[24] The C/O ratio and average size of the GO sheets increased as the oxidation temperature decreased. Thus, more functional groups and defect sites were created at higher oxidation temperature. For the preparation of large size GO, lower temperature reactions were favorable. Zhang *et al.* studied the effect of oxidation time and the amount of oxidants on the size control of GO sheets produced by chemical exfoliation.[25] With more reaction time and oxidants, the average size of the GO sheets exhibited a Gaussian distribution. In brief, as expected, higher temperature reactions, longer oxidation time, and more oxidant will reduce the GO particle size and decrease the conjugate structure domains.

The Dimiev–Tour model for the synthesis of GO has been adopted widely for understanding the formation of graphite oxide:[26,27] (i) transform graphite into a graphite intercalation compound (GIC) with H_2SO_4 intercalated into the graphite layers to enlarge the interlayer distance of graphite and form $C_{(21-28)}^{+}HSO_4^{-}\cdot 2H_2SO_4$; (ii) oxidants enter further into the graphite layers and react with the C atoms on the basal plane to produce functional groups; and (iii) moisture enters the graphite interlayers and ions exchange with HSO_4^{-} or SO_4^{2-} to form graphite oxide.

As illustrated in the Dimiev–Tour model, water actually played an essential role in the chemical reactions leading to the formation of GO. However, there has been no specific study reported in the literature using controlled experiments to examine the effects of water on the formation and production of GO.

In this study, we designed controlled experiments to investigate the effects of water content in the reactions and especially its effects on the formation and concentration of structural defects and carbonyl groups that were produced in the reactions. In addition, we propose a serial molecular models for understanding the dynamic processes involving $C_{(21-28)}^{+}HSO_4^{-}\cdot 2H_2SO_4$ under the influence of manganese heptaoxide (Mn_2O_7). We have also examined the role of water molecules in affecting the physical and chemical properties of GO, including altering the distribution of functional groups, the inter-layer spacing, the formation of structural defects, and the solution stability.

2. Experimental

2.1 Chemical reagents

The starting materials included graphite powders (<15 μm), sulfuric acid (H_2SO_4, 99%), potassium permanganate ($KMnO_4$, 98%), hydrogen peroxide (H_2O_2, 30%), hydrochloric acid (HCl, 37%), sodium nitrate ($NaNO_3$, 98%), and hydrazine hydrate ($N_2H_4\cdot H_2O$, 80 wt%) and they all were purchased commercially.

2.2 Materials characterization

X-ray photoelectron spectra (XPS) were recorded with (Thermo) ESCALAB 250XI. Raman spectra were recorded with HORIBA Scientific LabRAM HR Evolution with 514 nm laser. The zeta potentials of aqueous GO dispersions were measured with ZS90 Microelectrophoresis. X-ray diffraction (XRD) was carried out by using WJGS-009 D8 Advance X-ray diffractometer with Cu-K_α radiation (λ = 0.15418 nm, Bruker, Germany). UV-visible absorption spectra were taken with TU-1810 UV-visible spectrometer (PuXi, China). Transmission electron microscopy (TEM) images were taken with FEI Tecnai G2 F20 S-TWIN.

2.3 Synthesis of materials

2.3.1 Preparation of sulfuric acid with different concentrations. Six clean flasks were prepared, labeled 1, 2, 3, 4, 5, and 6, respectively. Appropriate amount of deionized water was then added into each flask, followed by 240 ml of H_2SO_4 (99%), to obtain H_2SO_4 of different concentrations (99%, 97%, 95%, 93%, 91%, and 89%). Since H_2SO_4 could absorb the water generated during oxidation, the reactions were conducted in an anhydrous atmosphere.

2.3.2 Preparation of GO. Basing on the previous studies, we selected a reaction temperature of 20 °C, reaction time of 48 h, and oxidant dosage of 5 times (5 equivalent of graphite) to prepare GO. The preparation of GO was carried out using a modified Hummers method,[13] in which GO was prepared by oxidation of natural graphite powders and H_2SO_4. In brief, graphite powders (6.0 g) were first placed in each flask under stirring in an ice bath. Under vigorous agitation, $KMnO_4$ (30.0 g) was added slowly while keeping the temperature of the suspension lower than 2 °C. Successively, the flask was transferred to a water bath of temperature 20 ± 2 °C and stirred continuously for about 48 h. 150 ml of water was then added into the solution and it was stirred for an additional 5 min. 20 ml of H_2O_2 was then added, after which the color of the solution would turn from dark brown to bright yellow. At last, additional 380 ml of water was added into the flask to obtain GO. The suspension was labeled as sGO-1, sGO-2, sGO-3, sGO-4, sGO-5, and sGO-6. In visual inspection, we found that sGO-1 and sGO-4 had the greatest difference in color, as shown in Fig. 1A. sGO-1 was the darkest in color and sGO-4 was bright yellow.

Each mixture was washed with HCl aqueous solution (5%, 800 ml, 200 ml each for 4 times) to remove the metal ions. They were then washed with deionized water until the supernatant became neutral. As the pH value increased, the hydrophilicity of GO increased. The process of washing required centrifugation to separate GO and supernatant. The centrifuge speed was set as 8000 rpm. Finally, the GO colloid was dried in a freeze dryer. The solid GO was labeled GO-1, GO-2, GO-3, GO-4, GO-5, and GO-6 in turn.

2.3.3 Reduction of GO. The color difference between sGO-1 and sGO-4 was the most obvious and they were selected to examine the effects of water in the reduction reactions. 100 ml suspension with GO concentration of 1 g l^{-1} was prepared for GO-1 and GO-4, respectively. They were sonicated for 1 h to exfoliate GO fully, then added 97 μl of hydrazine hydrate (80 wt%) and stirred to allow reactions at 85 ± 2 °C for 24 h. Finally, the solution was filtered and dried in vacuum. The reduced GO was labeled as rGO-1 and rGO-4, respectively.

3. Results and discussion

The carbon to oxygen ratio (C/O) would affect significantly the color of the GO suspension.[14] The color of suspension is light

green for a C/O ratio of 2.8–3.0. The color becomes yellowish green by further decreasing the C/O ratio. A bright yellow color was observed at the lowest C/O ratio of 2.0–2.4. In our experiment, we observed that GO-1 was khaki and GO-4 was bright yellow as displayed in Fig. 1 A.

The C/O ratios of GO-1 (Fig. 1C) and GO-4 (Fig. 1D) were obtained from XPS measurements and they were 1.73 and 1.69, respectively, indicating a similar degree of oxidation. The C1s spectrum of GO revealed four types of carbon bonds: C=C (284.8 eV), C–O (286.9 eV including epoxy/hydroxyls), C=O (287.8 eV), and O–C=O (289.1 eV).[28–30] Both GO samples had the same types of chemical bonds, *i.e.*, the functional groups were the same. However, the concentrations of the chemical bonds were different, indicating that the content of functional groups was different. The areal fractions of the peak for the four functional groups in GO-1 (Fig. 1C) were 33.6% (C=C), 25.5% (C–O), 32.0% (C=O), and 8.8% (O–C=O). On the other hand, the areal fractions of the peak for the four functional groups in GO-4 (Fig. 1D) were 32.6% (C=C), 30.6% (C–O), 26.1% (C=O), and 8.6% (O–C=O). The ratio of peak areas for the C–O (25.5%) bond and C=O (32.0%) bond in GO-1 (Fig. 1C) was 0.80, while the corresponding ration for GO-4 (Fig. 1D) was 1.17 (30.6%/26.1%). This significant difference indicates that the relative proportion of C–O bonds in GO-4 increased in comparison with that in GO-1, because GO-1 has been over-oxidized and part of the epoxy or hydroxyl groups were converted to carbonyls. The π–π conjugated structure in the graphene plane of GO-4 could have been destroyed by the introduced hydroxyl and epoxy functional groups. As a result, GO-1 has more residual π–π conjugated structures than GO-4, resulting in a lighter color than GO-1. At the same time, the carboxyl functional groups (O–C=O) in GO-1 and GO-4 would also contribute to the improved stability of the GO suspensions.[31]

The C/O ratio in rGO-1 (ESI, Fig. S1A†) and rGO-4 (ESI, Fig. S1B†) is 9.4 and 10.7, respectively. Using hydrazine hydrate to reduce GO, the hydroxyl and epoxy groups (C–O) could be removed easily, but the carbonyl groups (C=O) could hardly be removed.[22] These results indicate that more carbonyl groups remained in rGO-1 and more carbonyl groups were produced in GO-1. In Fig. 1B, using C=C as the standard, the C1s peak in XPS of GO-1 and GO-4 were normalized. The peak at 278 eV for GO-4 is sharper than GO-1, indicating that GO-4 had a more regular structure.[23,32]

We also characterized the GO samples with X-ray diffraction (XRD) that were prepared with different concentrations of H_2SO_4. No graphitic (002) peak was observed in all samples, indicating that all graphite samples had been oxidized completely.[33] However, noticeable differences were observed in the GO samples prepared from different concentrations of H_2SO_4 in the characteristic interlayer spacing between the graphene layers. As shown in Fig. 2B, GO-4, prepared with 93% H_2SO_4, exhibited the largest interlayer spacing ($d = 0.91$ nm, 2θ

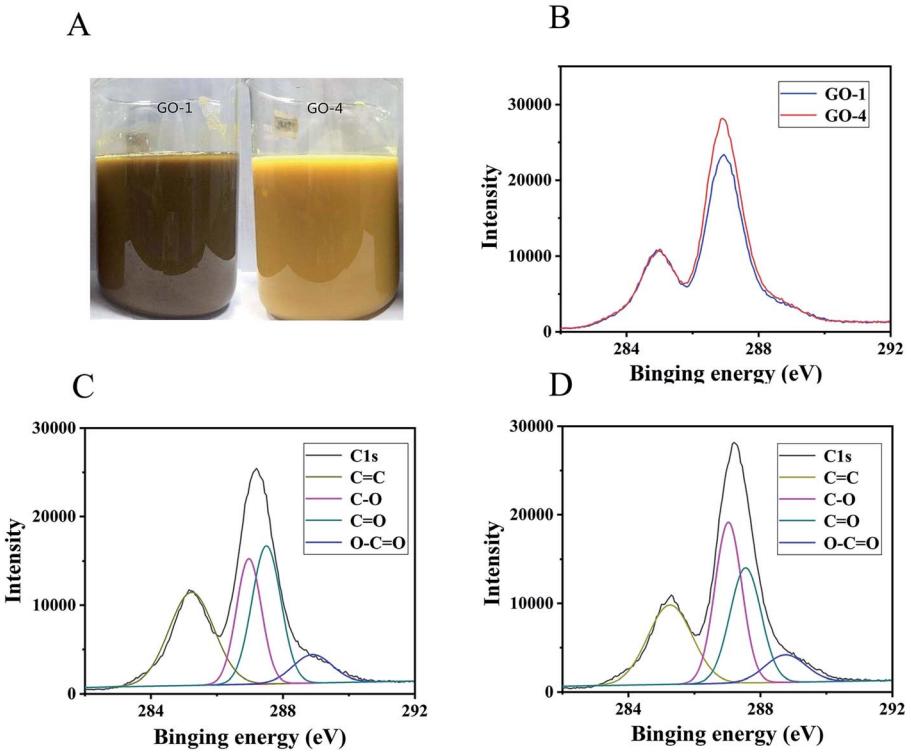

Fig. 1 (A) Color of GO-1 and GO-4 suspensions. (B) C1s XPS spectra of GO-1 and GO-4 normalized with respect to the C=C peak. It shows that the apparent peak for GO-4 at 287 eV is sharper than GO-1. (C and D) XPS data of GO-1 and GO-4. The areal ratio under the peak for C–O single bond and C=O double bond in GO-1 (C) was 0.80. The corresponding value for GO-4 (D) was 1.17. Water molecules increased the fraction of C–O bond.

= 9.7°), in contrast to the reduced interlayer spacing observed in GO-1 ($d = 0.86$ nm, $2\theta = 10.3°$) which was prepared with 99% H_2SO_4.

Hwee *et al.* compared the GO samples prepared by different methods and showed a variation in the spacing between the graphene layers. GO prepared using the Hummers method exhibited the largest inter-layer spacing (0.81 nm) and the lowest C/O ratio (1.12). GO prepared using the Hofmann method had an interlayer spacing of 0.72 nm and C/O ratio of 1.77. The smallest interlayer spacing of 0.70 nm was observed in GO prepared by the Staudenmaier method that had a C/O ratio of 2.52. These results showed that the lower the C/O ratio, the larger the interlayer spacing. However, since GO-1 and GO-4 samples had nearly the same C/O ratio, the difference in the interlayer spacing of the GO layers is attributed to the difference in the concentration of functional groups. As described in the established structure of GO, an epoxy group on the graphitic basal plane, the oxygen atom is 0.19 nm above the carbon grid (graphene).[34] On the other hand, a hydroxyl group on the same graphitic basal plane, the top hydrogen atom is 0.22 nm above the carbon grid.[34] C and O atoms in epoxy and hydroxyl groups are in the hybrid sp^3 configuration.[35] The C and O atoms in the carbonyl functional group are planar sp^2-hybridized, contributing less to the expansion of the interlayer spacing. As a result, we suggest that GO-4 had a larger interlayer spacing than GO-1 because GO-4 contained more epoxy groups and hydroxyl groups than GO-1. In brief, the number of epoxy groups and hydroxyl groups played significant roles in governing the interlayer spacing. When the interlayer spacing was reduced, it should indicate that the amount of epoxy and hydroxyl groups in the product was reduced accordingly.

Raman spectroscopy was applied to analyze the G-band and D-band characteristic of graphitic structure. The G-band is associated with graphitic carbons and the D-band is related to the structural defects or partially disordered graphitic domains.[36] The Raman spectra of GO showed the G-band at ~1600 cm^{-1} and D-band at ~1350 cm^{-1}.[37,38] The intensity ratio (I_D/I_G) for GO-1 (Fig. 3A) is 1.02 and the corresponding I_D/I_G ratio for GO-4 is 0.89 as shown in Fig. 3B. The comparative data indicated that there were more structural defects and lattice distortions in GO-1 than GO-4. In the process of peroxidation reaction between some hydroxyl and carboxyl functional groups to form carbonyl, new structural defects were formed, which led to the enhancement of the D peak in GO-1. The intensity ratio (I_D/I_G) for rGO-1 (Fig. 3C) is 1.30, which is also lower than that for rGO-4 as shown in Fig. 3D with I_D/I_G ratio of 1.68. These results indicate that there were more structural defects in rGO-4 than rGO-1. During the reduction process, GO-4 contained more hydroxyl and epoxy groups than GO-1. As more reduction reactions occurred, more structural defects were produced. The intensity of the 2D peak in GO-4 is greater than that in GO-1, indicating that the number of graphene layers in the graphite flakes in GO-4 is smaller than that in GO-1. Thicker graphite flakes resulted in the darker color of the GO-1 suspension. On the other hand, GO-1 and GO-4 contained different functional groups. GO-1 had more carbonyl groups on the edges and retained more conjugations in the basal plane, which is another reason that led to the darker color of the GO-1 suspension.

The UV-vis spectra of the GO suspensions are associated with the $\pi \rightarrow \pi^*$ transitions and $n \rightarrow \pi^*$ transitions.[39,40] As shown in Fig. 4, the maximum wavelength of absorption of GO-1 is 229 nm and the maximum wavelength of absorption of GO-4 is 231 nm. Compared with the GO-1 suspension, the GO-4 absorption spectra were slightly blue-shifted. The spectra suggest that the more π–π conjugations in GO-1 were due to the greater retention of carbon rings in the basal planes. The electronic transition of the C=C double bond in graphite is the $\pi \rightarrow \pi^*$ transition. When more oxygen atoms are attached onto the graphitic basal plane of GO-1, part of the electronic transition mode became the $n \rightarrow \pi^*$ transition. Since the $n \rightarrow \pi^*$ transition energy is less than the $\pi \rightarrow \pi^*$ transition, so the absorption band is slight blue-shifted. It showed that as more oxygen atoms were introduced into the basal plane of GO-4, GO-4 would have more hydroxyl and epoxy groups than GO-1. The spectrum has a shoulder peak at 300 nm, which is attributed to the $n \rightarrow \pi^*$ transition of C=O bonds.[39]

As illustrated in Fig. 4 (inset), a comparison of the GO suspensions with the same concentration, the color of the GO-1 suspension is darker than that of the GO-4 suspension. GO-4 had more hydroxyl and epoxy groups introduced in the basal

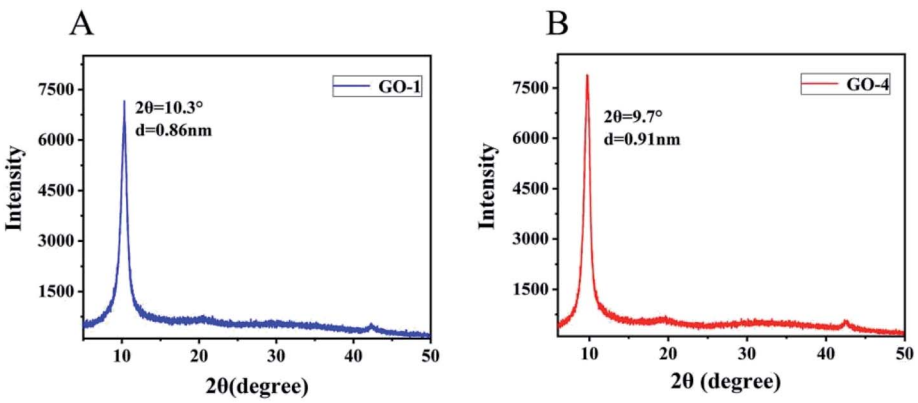

Fig. 2 XRD pattern of (A) GO-1 and (B) GO-4. The interlayer spacing of GO-1 is 0.86 nm. The interlayer spacing of GO-4 is 0.91 nm.

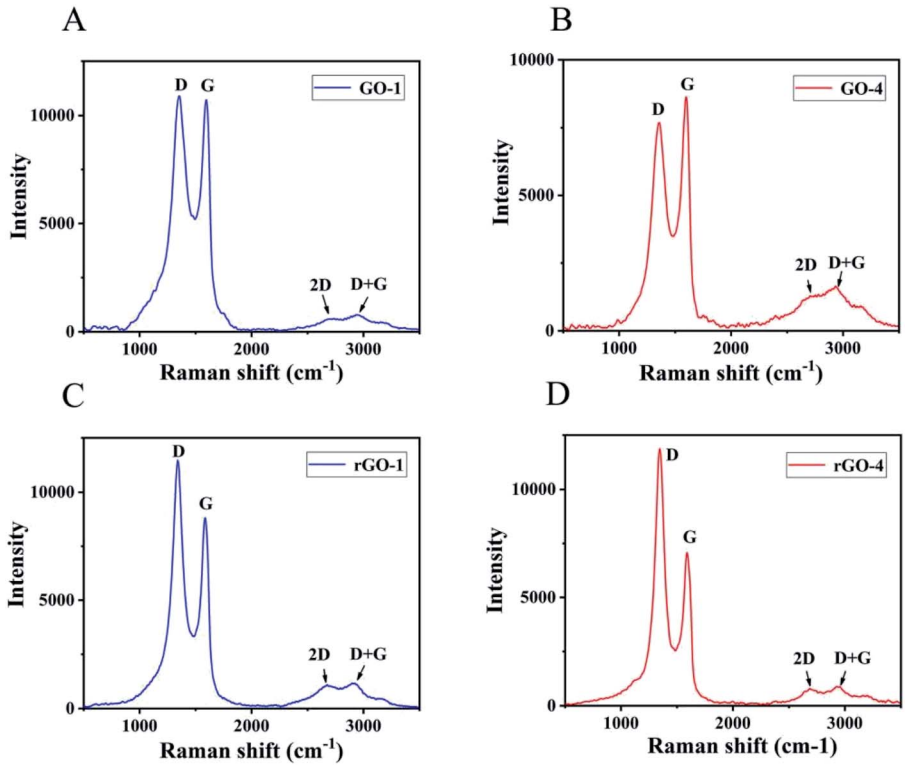

Fig. 3 Raman spectra excited with laser of wavelength 514 nm. (A) GO-1, (B) GO-4, (C) rGO-1, and (D) rGO-4. The intensity ratio (I_D/I_G) is 1.02 for GO-1, 0.89 for GO-4, 1.30 for rGO-1, and 1.68 for rGO-4.

plane than GO-1 and there were fewer π–π conjugations remained in the basal plane, resulting its color is lighter than the GO-1 suspension. On the other hand, GO-4 has fewer graphene layers than GO-1, a factor that also made the color lighter than the GO-1 suspension.

The suspensions of GO were negatively charged, mainly due to the carboxyl groups at the edges of the GO sheets.[41] The zeta potentials of GO-1 and GO-4 suspensions (0.04 mg ml^{-1}) were measured to be −42.3 mV and −44.5 mV, respectively, and they were negatively charged, indicating that they had carboxyl groups on the edges. Their values are all lower than −30 mV, so they all had good dispersibility.[42] The GO-1 suspension has a slightly higher zeta potential than that of the GO-4 suspension, indicating that GO-4 is more stable and has more carboxyl groups.

By comparison, the 1.0 mg ml^{-1} suspension of GO-1 can be stored stably for three weeks, while the GO-4 solution could be stored stably for four weeks. (ESI, Table S1†).

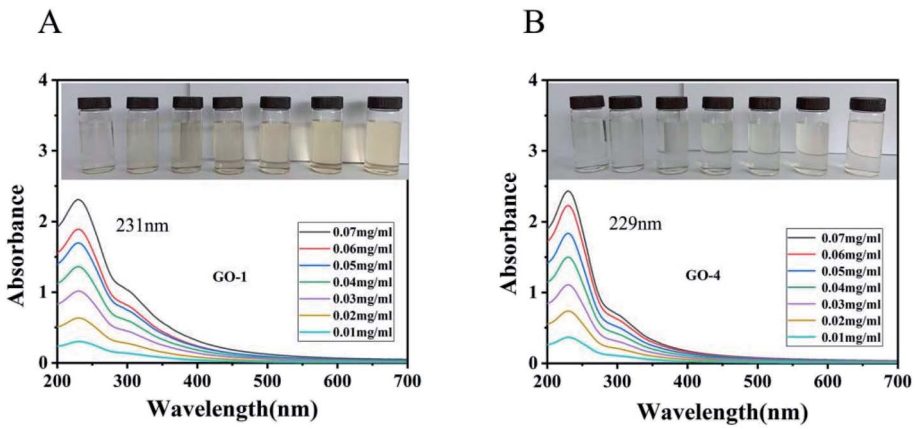

Fig. 4 UV-vis absorption spectra of different (A) GO-1 suspensions and (B) GO-4 suspensions. Inset shows the color of the suspensions with different concentrations of GO (concentration increased from 0.01 to 0.07 mg ml^{-1} from left to right). The maximum wavelength of absorption of GO-1 is 231 nm and the maximum wavelength of absorption of GO-4 is 229 nm.

When observed in TEM (Fig. 5) and SEM (ESI, Fig. S2†), the GO-1 and GO-4 samples showed a similar morphology. Their corresponding electron diffraction patterns (Fig. 5C and D) revealed that both retained excellent single crystalline structure without noticeable structural degradation due to the oxidation reactions. In fact, both GO-1 and GO-4 could be easily exfoliated into single layer GO with ultrasonic treatment.

Thermogravimetric analysis (TGA) of GO-1 and GO-4 (Fig. 6) exhibited similar features: a weight loss before 100 °C is resulted from the releasing of trapped water between GO sheets.[43] The curve at this stage shows that both have the same moisture content. The sharp weight loss between 200 and 230 °C is attributed to the decomposition of less stable oxygenic functional groups on the GO sheets.[44] A gradual mass loss in the range of 230–800 °C is related to the removal of more stable functional groups, including part of the hydroxyl groups and carbonyl groups.[45] After pyrolysis, the remaining mass of GO-4 is more than that of GO-1, indicating that the thermal stability of GO-4 is better than GO-1.

To further understand the reaction mechanism of GO, we propose a series of molecular models for the involved reactions. The first model (Fig. 7A) is assumed to start with GIC. When another HSO_4^- group intercalates into the graphite basal plane, the original HSO_4^- group will generate steric hindrance to hinder the continued insertion of the HSO_4^- group. On the other hand, when a water molecule is present, part of the water would ionize to form hydrogen ions (H^+) and hydroxide ions (OH^-). In order to reduce the steric hindrance, in Route 1 and Route 2, part of the HSO_4^- groups on the graphite plane could exchange with the hydroxides, generating hydroxyl groups as illustrated in Fig. 7B and H_2SO_4. The hydroxyl group has a smaller mass and volume than the HSO_4^- group, so the resulting steric hindrance is reduced. Then the next HSO_4^- groups can intercalate into the graphite plane more easily. The

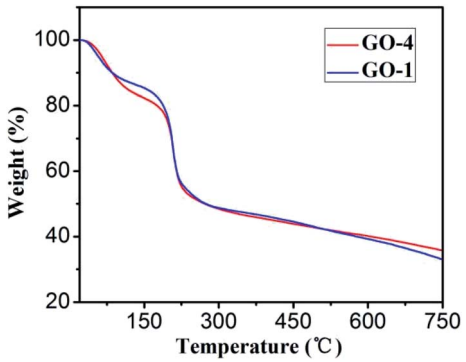

Fig. 6 TGA analysis of GO-1 (blue) and GO-4 (red) samples.

newly formed H_2SO_4 can slow down the decrease of H_2SO_4 concentration in the oxidation reaction.

In Route 1, if another intercalated HSO_4^- group is adjacent to the original hydroxyl (OH^-) group (Fig. 7C1), the newly inserted HSO_4^- group could react with water, generating a hydroxyl group (Fig. 7D1). Eventually, two adjacent hydroxyl groups (OH^-) could react and lose a water molecule to form an epoxy group. In Route 2, if the newly intercalated HSO_4^- group is relatively far away from the original hydroxyl group, it could also react with water to produce a new hydroxyl group (Fig. 7D2), but the new hydroxyl group may not react with the original hydroxyl group (OH^-) to produce an epoxy group. Therefore, in Route 1 the GIC are more likely to form epoxy groups. In Route 2, GIC are more likely to form hydroxyl groups.

If the reaction uses 99% H_2SO_4, there is little moisture in the system, the migration of the particles would be slow, and the hydroxyl ions were difficult to form in the system. In the model of GIC (Fig. 7A), the HSO_4^- group cannot exchange with hydroxyl (OH^-). In Route 4, the large steric hindrance could

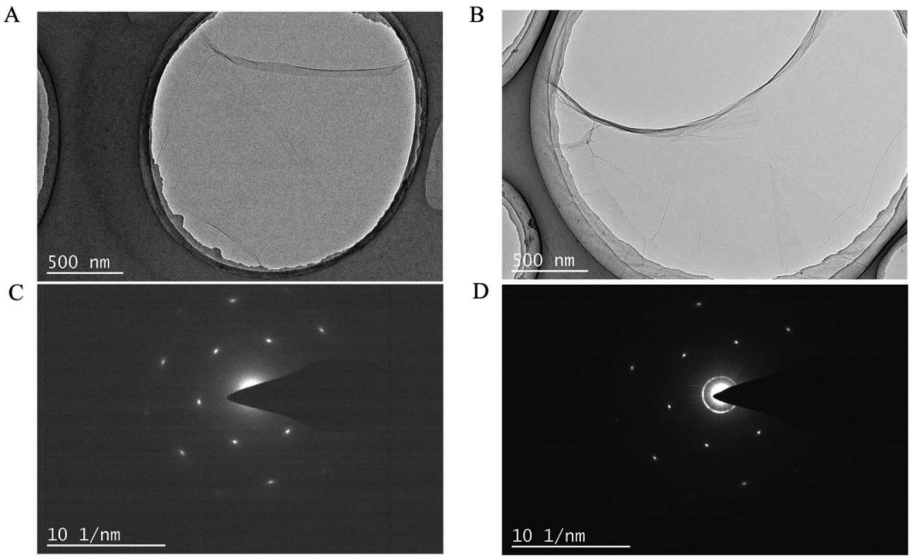

Fig. 5 TEM images of (A) GO-1 and (B) GO-4 showing similar morphology and corresponding electron diffraction pattern of (C) GO-1 and (D) GO-4 showing single crystallinity of the GO sheets.

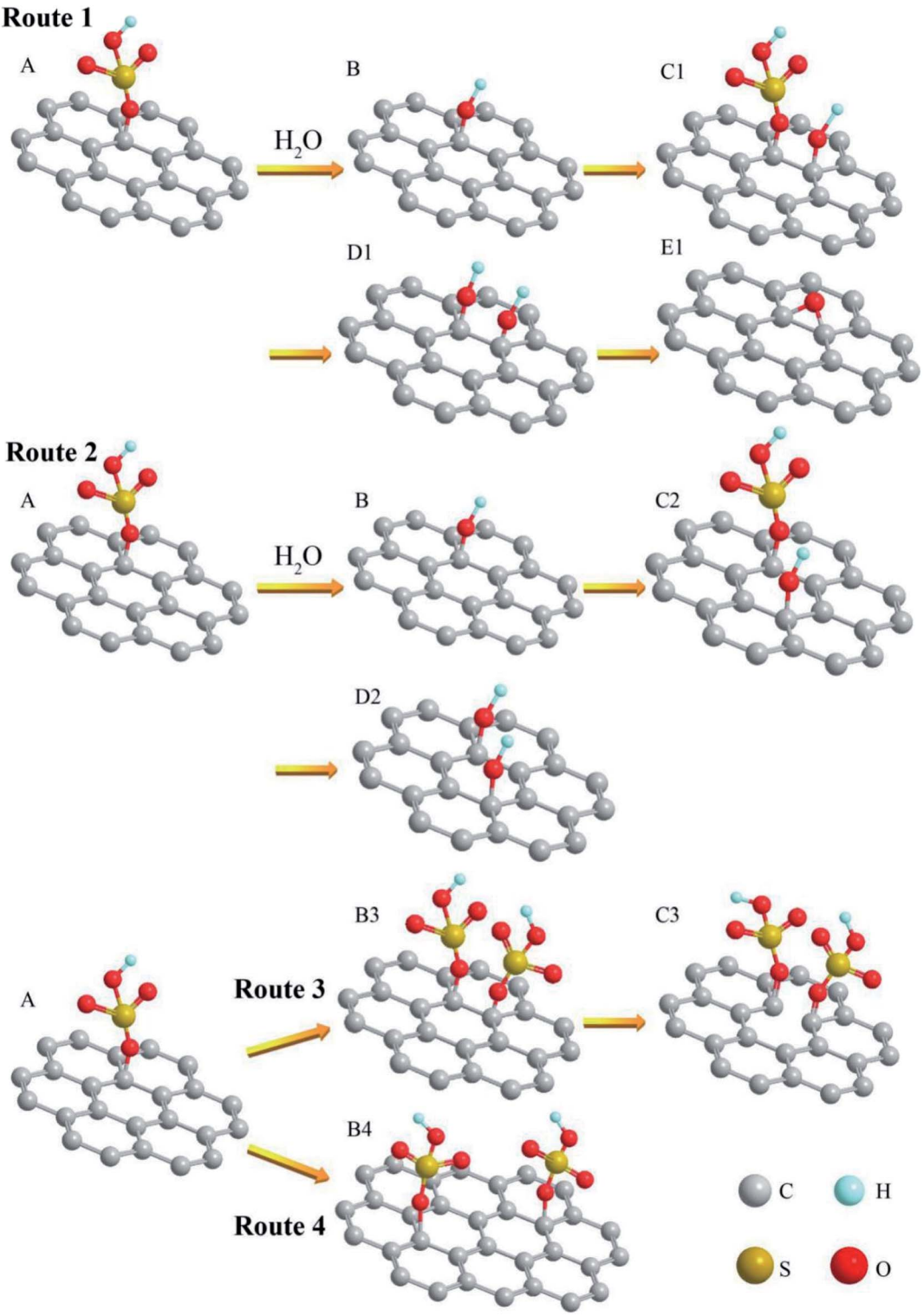

Fig. 7 Structural changes of GIC oxidation reaction. Route 1 and 2 are oxidation processes with a proper amount of water in the system. After the OH^- replaces HSO_4^-, the steric hindrance is reduced, which is beneficial for more HSO_4^- to enter the graphitic carbon layer. Route 3 and 4 are oxidation processes in anhydrous systems. Due to steric hindrance, more carbonyl groups (C=O) and defects are generated.

allow another HSO_4^- group to be intercalated away from the original HSO_4^- group (Fig. 7B4). Eventually it could lead to a decrease in the number of HSO_4^- groups on the graphite basal plane. The corresponding number of hydroxyl groups in GO is therefore reduced. In another case (Route 3), the next HSO_4^- group is intercalated into adjacent C atom (Fig. 7B3), the C–C bonds are likely broken by the action of steric hindrance and oxidant. Structural defects (Fig. 7C3) are therefore generated on

the graphitic plane. These defects could even help form edges and are easy to produce carbonyl groups.

During the formation of graphite oxide, diamanganese heptaoxide (Mn_2O_7) served as the oxidizing agent that is created in the following reactions[46]

$$KMnO_4 + 3H_2SO_4 \rightarrow K^+ + MnO_3^+ + 3HSO_4^- + H^+ + H_2O \quad (1)$$

$$KMnO_4 \rightarrow K^+ + MnO_4^- \quad (2)$$

$$MnO_3^+ + MnO_4^- \rightarrow Mn_2O_7 \quad (3)$$

$$Mn_2O_7 + H_2O \rightarrow 2HMnO_4 \quad (4)$$

In reaction (1), water (H_2O) is produced. In reaction (3), Mn_2O_7 is produced from the reaction between MnO_3^+ and MnO_4^-. The bimetallic heptoxide is far more oxidizing than monometallic tetraoxide.[47]

Another effect of water molecules in the reaction is also the reason why GO-1 is different from GO-4. Manganese heptaoxide (Mn_2O_7) can react with water to regenerate permanganic acid ($HMnO_4$). Permanganic acid ($HMnO_4$) and manganese trioxide (MnO_3^+) can also react to produce manganese heptaoxide (Mn_2O_7). The water molecules can adjust the ratio of various oxidants in the reaction, so that the oxidants of the entire reaction are in a dynamic equilibrium, preventing excessive oxidation of graphite to produce carbonyl groups. Therefore, GO-1 prepared with an anhydrous reaction has a higher carbonyl ratio than GO-4.

4. Conclusions

The water molecules in H_2SO_4 have a significant effect on the oxidation of graphite in the preparation of graphene oxide. The water molecule is more conducive to the oxidation of graphite to produce epoxy and hydroxyl functional groups, while reducing the occurrence of structural defects. These results suggest that the 93% H_2SO_4 could disrupt the basal plane of the graphite less than 99% H_2SO_4. As a result, GO obtained with 93% H_2SO_4 shows best properties, such as solubility and stability. According to the XRD analysis, GO obtained with 93% H_2SO_4 also has the largest (0.91 nm) average interlayer spacing. The Raman analysis showed the I_D/I_G ratio for GO-4 obtained with 93% H_2SO_4 is lower than GO-1 obtained with 99% H_2SO_4, indicating a less defective structure of GO-4.

Conflicts of interest

There are no conflicts to declare.

References

1 A. K. Geim and K. S. Novoselov, *Nat. Mater.*, 2007, **6**, 183–190.
2 Y. Xu and G. Shi, *J. Mater. Chem.*, 2011, **21**, 3311–3323.
3 J. Zhang, T. Tian, Y. Chen, Y. Niu, J. Tang and L. C. Qin, *Chem. Phys. Lett.*, 2014, **591**, 78–81.
4 S. Guo, Y. Zhang, Y. Ge, S. Zhang, H. Zeng and H. Zhang, *Adv. Mater.*, 2019, **31**, 1902352.
5 J. Pei, J. Yang, Y. Tanju, H. Zhang and Y. Lu, *Adv. Mater.*, 2017, **31**, 1706945.
6 J. He, L. Tao, H. Zhang, B. Zhou and J. Li, *Nanoscale*, 2019, **11**, 2577–2593.
7 D. R. Dreyer, S. Park, C. W. Bielawski and R. S. Ruoff, *Chem. Soc. Rev.*, 2009, **39**, 228–240.
8 O. C. Compton and S. B. T. Nguyen, *Small*, 2010, **6**, 711–723.
9 D. R. Dreyer, A. D. Todd and C. W. Bielawski, *Chem. Soc. Rev.*, 2014, **43**, 5288–5301.
10 L. G. Guex, B. Sacchi, K. Peuvot, R. L. Andersson and R. T. Olsson, *Nanoscale*, 2017, **9**, 9562–9571.
11 D. A. Dikin, S. Stankovich, E. J. Zimney, R. D. Piner, G. H. B. Dommett, G. Evmenenko, S. T. Nguyen and R. S. Ruoff, *Nature*, 2007, **448**, 457–460.
12 B. C. Brodie, *Philos. Trans. R. Soc. London*, 1859, **149**, 249–259.
13 W. S. Hummers and R. E. Offeman, *J. Am. Chem. Soc.*, 1958, **208**, 1334–1339.
14 S. Shamaila, A. K. L. Sajjad and A. Iqbal, *Chem. Eng. J.*, 2016, **294**, 458–477.
15 V. V. Avdeev, L. A. Monyakin, I. V. Nikol'skay, N. E. Sorokin and K. N. Semenenko, *Carbon*, 1992, **30**, 819–823.
16 P. V. Lakshminarayanan, H. Toghiani and C. U. Pittman Jr, *Carbon*, 2004, **42**, 2433–2442.
17 N. Zhang, L. Y. Wang, H. Liu and Q. K. Cai, *Surf. Interface Anal.*, 2010, **40**, 1190–1194.
18 Y. Kopelevich and P. Esquinazi, *Adv. Mater.*, 2007, **19**, 4559–4563.
19 A. A. Balandin, S. Ghosh, W. Bao, I. Calizo, D. Teweldebrhan, F. Miao and C. N. Lau, *Nano Lett.*, 2008, **8**, 902–907.
20 S. F. Pei and H. M. Cheng, *Carbon*, 2012, **50**, 3210–3228.
21 S. Stankovich, D. A. Dikin, R. D. Piner, K. A. Kohlhaas, A. Kleinhammes, Y. Jia, Y. Wu, S. B. T. Nguyen and R. S. Ruoff, *Carbon*, 2007, **45**, 1558–1565.
22 X. Gao, J. Jang and S. Nagase, *J. Phys. Chem. C*, 2010, **114**, 832–842.
23 D. C. Marcano, D. V. Kosynkin, J. M. Berlin, A. Sinitskii, Z. Sun, A. Slesarev, L. B. Alemany, W. Lu and J. M. Tour, *ACS Nano*, 2010, **4**, 4806–4814.
24 D. W. Kang and H. S. Shin, *Carbon Lett.*, 2012, **13**, 39–43.
25 L. Zhang, J. Liang, Y. Huang, Y. Ma, Y. Wang and Y. Chen, *Carbon*, 2009, **47**, 3365–3368.
26 A. M. Dimiev, S. M. Bachilo, R. Saito and J. M. Tour, *ACS Nano*, 2012, **6**, 7842–7849.
27 P. C. Eklund, C. H. Olk, F. J. Holler, J. G. Spolar and E. T. Arakawa, *J. Mater. Res.*, 1986, **1**, 361–367.
28 T. Szabó, O. Berkesi, P. Forgó, K. Josepovits, Y. Sanakis, D. Petridis and I. Dékány, *Chem. Mater.*, 2006, **18**, 2740–2749.
29 H. He, T. Riedl, A. Lerf and J. Klinowski, *J. Phys. Chem.*, 1996, **100**, 19954–19958.
30 L. Peng, Z. Xu, Z. Liu, Y. Wei, H. Sun, Z. Li, X. Zhao and C. Gao, *Nat. Commun.*, 2015, **6**, 5716.
31 J. T. Robinson, F. K. Perkins, E. S. Snow, Z. Wei and P. E. Sheehan, *Nano Lett.*, 2008, **8**, 3137–3140.

32 Y. Aoi, K. Ono and E. Kamijo, *J. Appl. Phys.*, 1999, **86**, 2318–2322.
33 Q. Du, M. Zheng, L. Zhang, Y. Wang and J. Cao, *Chem. Res.*, 2010, **55**, 3897–3903.
34 H. C. Schniepp, JeL. Li, M. J. McAllister, H. Sai, M. HerreraAlonso, D. H. Adamson, R. K. Prud'homme, R. Car, D. A. Saville and I. A. Aksay, *J. Phys. Chem. B*, 2006, **110**, 8535–8539.
35 C. Gómez-Navarro, J. C. Meyer, R. S. Sundaram, A. Chuvilin and U. Kaiser, *Nano Lett.*, 2010, **10**, 1144–1148.
36 K. N. Kudin, B. Ozbas, H. C. Schniepp, R. K. Prud'Homme, I. A. Aksay and R. Car, *Nano Lett.*, 2008, **8**, 36–41.
37 F. Tuinstra and J. L. Koenig, *J. Chem. Phys.*, 1970, **53**, 1126–1130.
38 G. Venugopal, M.-H. Jung, M. Suemitsu and S.-J. Kim, *Carbon*, 2011, **49**, 2766–2772.
39 J. Chen, Y. Li, L. Huang, C. Li and G. Shi, *Carbon*, 2015, **81**, 826–834.
40 Y. Xu, K. Sheng, C. Li and G. Shi, *J. Mater. Chem.*, 2011, **21**, 7376–7380.
41 I. Jung, D. A. Dikin, R. D. Piner and R. S. Ruoff, *Nano Lett.*, 2008, **8**, 4283–4287.
42 D. Li, M. B. Müller, S. Gilje, R. B. Kaner and G. G. Wallace, *Nat. Nanotechnol.*, 2008, **3**, 101–105.
43 S. Eigler, C. Dotzer, A. Hirsch, M. Enzelberger and P. Müller, *Chem. Mater.*, 2012, **24**, 1276–1282.
44 M. J. Mcallister, J.-L. Li, D. H. Adamson, H. C. Schniepp, A. A. Abdala, J. Liu, M. Herrera-Alonso, D. L. Milius, R. Car, R. K. Prud'Homme and I. A. Aksay, *Chem. Mater.*, 2007, **19**, 4396–4404.
45 V. Agarwal and P. Zetterlund, *Chem. Eng. J.*, 2020, **405**, 127018.
46 K. R. Koch, *J. Chem. Educ.*, 1982, **59**, 973–974.
47 A. Simon, R. Dronskowski, B. Krebs and B. Hettich, *Angew Chem. Int. Ed. Engl.*, 1987, **26**, 139–140.